Pergamon

Geochimica et Cosmochimica Acta, Vol. 66, No. 18, pp. 3247–3262, 2002
Copyright © 2002 Elsevier Science Ltd
Printed in the USA. All rights reserved
0016-7037/02 $22.00 + .00

PII S0016-7037(02)00928-6

Influence of Mn oxides on the reduction of uranium(VI) by the metal-reducing bacterium *Shewanella putrefaciens*

JAMES K. FREDRICKSON,[1,*] JOHN M. ZACHARA,[1] DAVID W. KENNEDY,[1] CHONGXUAN LIU,[1] MARTINE C. DUFF,[2,†] DOUGLAS B. HUNTER[2,†] and ALICE DOHNALKOVA[1]

[1]Pacific Northwest National Laboratory, Richland, WA 99352, USA
[2]Westinghouse Savannah River Company, Savannah River Technology Center, Aiken, SC 29808, USA

(*Received October* 12, 2001; *accepted in revised form April* 29, 2002)

Abstract—The potential for Mn oxides to modify the biogeochemical behavior of U during reduction by the subsurface bacterium *Shewanella putrefaciens* strain CN32 was investigated using synthetic Mn(III/IV) oxides (pyrolusite [β-MnO_2], bixbyite [Mn_2O_3] and K^+-birnessite [$K_4Mn_{14}O_{27} \cdot 8H_2O$]). In the absence of bacteria, pyrolusite and bixbyite oxidized biogenic uraninite (UO_2[s]) to soluble U(VI) species, with bixbyite being the most rapid oxidant. The Mn(III/IV) oxides lowered the bioreduction rate of U(VI) relative to rates in their absence or in the presence of gibbsite ($Al[OH]_3$) added as a non-redox-reactive surface. Evolved Mn(II) increased with increasing initial U(VI) concentration in the biotic experiments, indicating that valence cycling of U facilitated the reduction of Mn(III/IV). Despite an excess of the Mn oxide, 43 to 100% of the initial U was bioreduced after extended incubation. Analysis of thin sections of bacterial Mn oxide suspensions revealed that the reduced U resided in the periplasmic space of the bacterial cells. However, in the absence of Mn(III/IV) oxides, UO_2(s) accumulated as copious fine-grained particles external to the cell. These results indicate that the presence of Mn(III/IV) oxides may impede the biological reduction of U(VI) in subsoils and sediments. However, the accumulation of U(IV) in the cell periplasm may physically protect reduced U from oxidation, promoting at least a temporal state of redox disequilibria. *Copyright © 2002 Elsevier Science Ltd*

1. INTRODUCTION

Dissimilatory metal-reducing bacteria (DMRB) couple the oxidation of organic matter or H_2 to the reduction of Fe(III) or Mn(III/IV) and are important catalysts in the linked cycling of C and metals in the environment (Nealson and Myers, 1992; Lovley, 1993; Nealson and Saffarini, 1994). At circumneutral pH, Fe(III) and Mn(III/IV) oxides are poorly soluble, yet they are accessible, to varying degrees, by respiring DMRB. The mechanisms by which microorganisms access metal oxides during respiration are not well understood. In metal-reducing bacteria such as *Shewanella oneidensis* strain MR-1, bioreduction may involve direct reduction by *c*-type cytochromes located in the outer membrane (OM) (Myers and Myers, 1992). Water-soluble quinone-like compounds that function as electron shuttles between the bacterial electron transport system and the oxides may also be important (Newman and Kolter, 2000). Regardless, it is clear that the reduction of metal oxides by DMRB is constrained to large degree by physical limitations imposed by the solid surface. The process is complex and is influenced, in addition to biologic factors, by mineral properties, including composition, degree of crystallinity and crystal disorder, microheterogeneities, surface area, and free energy constraints (Burdige et al., 1992; Roden and Zachara, 1996; Zachara et al., 1998).

In contrast to Fe and Mn, U typically exists as a highly soluble ion in oxidized, circumneutral groundwaters, typically as a U(VI) carbonate complex. U(VI) is readily reduced by DMRB under anoxic conditions, resulting in the precipitation of uraninite (UO_2[s]) (Lovley et al., 1991; Gorby and Lovley, 1992). The rapid rate of U(VI) reduction by DMRB (Truex et al., 1997) and the relatively low solubility of U(IV) makes bioremediation an attractive option for removing soluble U from contaminated groundwaters (Lovley and Phillips, 1992; Abdelouas et al., 1998). U cycling and the formation of U roll-front deposits may be due largely to the activity of metal-reducing bacteria (Mohagheghi et al., 1985; Lovley et al., 1991).

As part of previous investigations focused on examining the effects of Fe(III) oxides on bacterial reduction, U(VI) carbonate complexes ($UO_2[CO_3]_3^{4-}$[aq] and $UO_2[CO_3]_2^{2-}$[aq]) were reduced by *Shewanella putrefaciens* strain CN32 to U(IV) in the absence and presence of goethite (α-FeOOH[s]) (Fredrickson et al., 2000). Uranium(VI) was also reduced by bacterially reduced anthraquinone-2,6-disulfonate (AQDS), with AH_2DS being the reduced form in the absence of cells, and by Fe(II) sorbed to goethite in abiotic experiments. In the absence of goethite, uraninite was a major product of direct microbial reduction and reduction by AH_2DS. These results indicated that DMRB, via a combination of direct enzymatic or indirect mechanisms, reduce U(VI) to insoluble U(IV) in the presence of crystalline Fe(III). These results contrasted with those of Wielinga et al. (2000), who observed that ferrihydrite inhibited the bioreduction of U(VI) by *Shewanella algae* strain BrY. Such differences are likely caused by the contrasting bioavailability of Fe(III) in the poorly crystalline and crystalline state as controlled by solid-phase thermodynamics and interfacial elec-

* Author to whom correspondence should be addressed, at Pacific Northwest National Laboratory, MSIN P7-50, P.O. Box 999, Richland WA 99352.
† Formerly of the University of Georgia, Savannah River Ecology Laboratory, Aiken, SC 29802.

tron transfer kinetics. Subtle distinctions of this nature demonstrate the complexity of enzymatic metal reduction.

Given their high redox potentials (Robie et al., 1978), Mn(III/IV) oxides should be utilized as an electron acceptor before U(VI) during respiration coupled to organic carbon or H_2 oxidation. Among Mn(IV), Fe(III), and U(VI), Mn(IV) generally has the highest half-cell reduction potential, followed by Fe(III) and then U(VI), although the actual potentials are dependent upon chemical form, concentration, and other factors such as pH. However, differences in solubility and electron transfer kinetics could affect the relative utilization of these metals as electron acceptors. In addition, Mn(III/IV) oxides have the thermodynamic potential to oxidize U(IV). Mn(III/IV) and Fe(III) oxides coexist in many subsurface materials, including Pliocene fluvial sediments of the Ringold Formation on the U.S. Department of Energy's (DOE) Hanford Site in south central Washington (Zachara et al., 1995) and in soils and subsoils at the DOE's Oak Ridge Reservation in eastern Tennessee, where significant plumes of U(VI)-contaminated groundwaters exist (e.g., Swanson et al., 1999). Hence, the presence of these metal oxides has the potential to complicate remediation efforts that involve redox manipulation at these sites. Complex thermodynamic and kinetic considerations make it difficult to predict the behavior of U in soils or sediments containing Mn oxides that are being reduced as a result of microbial respiration. The purpose of this research, therefore, was to investigate the potential for Mn(III, IV) oxides to (a) oxidize biogenic UO_2(s) and (b) compete with U(VI)(aq) for electron equivalents liberated during the bacterial oxidation of H_2 or lactate by the dissimilatory metal-reducing bacterium *S. putrefaciens* CN32.

2. EXPERIMENTAL PROCEDURES

2.1. Bacteria, Media, and Minerals

S. putrefaciens CN32 was provided courtesy of Dr. David Boone (Subsurface Microbial Culture Collection, Portland State University, Portland, OR). CN32 was isolated from a subsurface core sample (250 m beneath the surface) from the Morrison Formation in northwestern New Mexico (Fredrickson et al., 1998). CN32 was routinely cultured aerobically in tryptic soy broth (TSB), 30 g L^{-1} (Difco Laboratories, Detroit, MI), and stock cultures were maintained by freezing in 40% glycerol at −80°C.

Batch experiments were conducted in 10 mL of 30 mmol/L, pH 7, bicarbonate buffer with H_2 (10 cm^3) or lactate (25 mmol/L) as electron donors and N_2:CO_2 (80:20) headspace. CN32 cells were harvested from TSB cultures at mid- to late log phase by centrifugation, washed twice with 30 mmol/L PIPES buffer and once with pH 7 bicarbonate buffer to remove residual medium. The cells were then suspended in bicarbonate buffer and purged with O_2-free N_2. Washed cells were added to obtain a final concentration of 2 to 4 × 10^8 cells mL^{-1}.

Well-crystallized pyrolusite (β-MnO_2, Fig. 1a) was synthesized by a modification of the method of Stahl and James (1991) and had a surface area of 0.9 m^2 g^{-1} as determined by multipoint Brunauer-Emmett-Teller analysis (Quantachrome Corp., Boynton Beach, FL). A K^+-birnessite ($K_4Mn_{14}O_{27} \cdot 8H_2O$) was synthesized by slowly adding a $KMnO_4$ solution to a basic solution of $MnCl_2$ (McKenzie, 1971). The X-ray diffraction (XRD) pattern (Fig. 1b) was characteristic of 0.7 nm birnessite and did not contain identifiable accessory phases (Fig. 1b). The precipitate was heated at 75°C for 18.5 h and washed and centrifuged with 200 mL of deionized water to remove excess chloride; its surface area was 47.9 m^2 g^{-1}. Bixbyite (Mn_2O_3, Fig. 1c) was generated as a result of our attempts to synthesize manganite (MnOOH) using the procedure of Mcardell et al. (1998). The bixbyite contained a hausmanite impurity (e.g., d = 4.927 Å at 19.2° 2θ) and exhibited a surface area of 26.7 m^2 g^{-1}. The XRD pattern of bixbyite (Fig. 1c) showed a relatively high base-

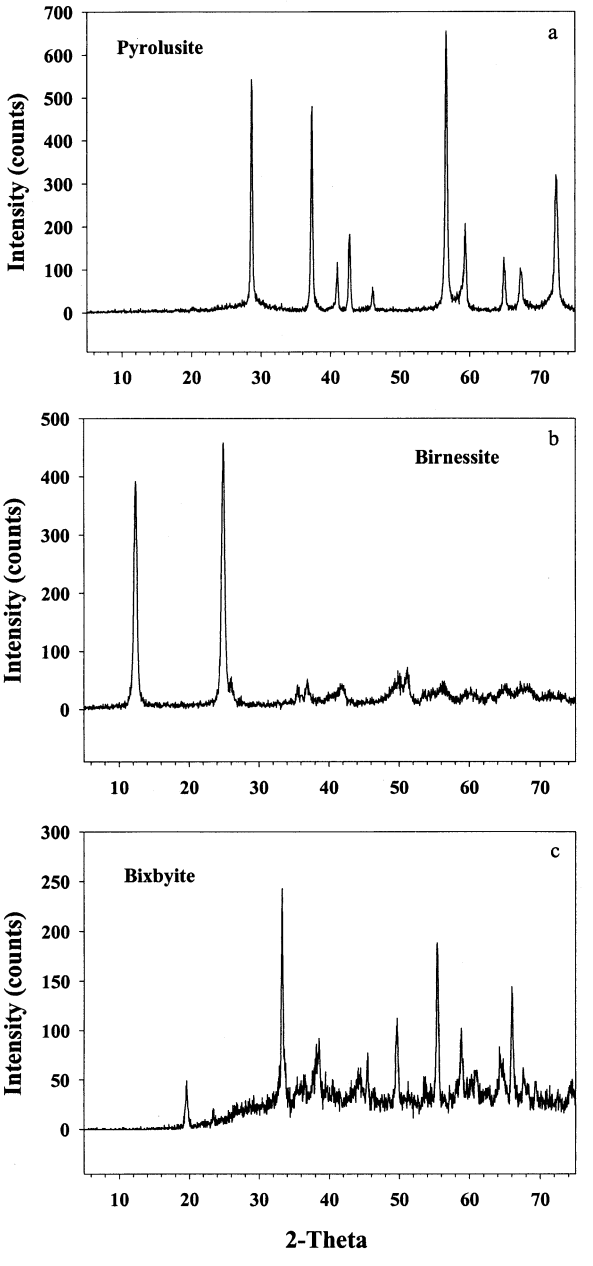

Fig. 1. X-ray diffractograms of the three synthetic Mn(III/IV) oxides: (a) pyrolusite, (b) birnessite, and (c) bixbyite.

line and signal-to-noise ratio, factors qualitatively indicative of structural disorder.

Uraninite (UO_2[s]) was synthesized by reducing uranyl acetate in bicarbonate buffer with *S. putrefaciens* CN32 and H_2 as the electron donor. The solids were collected and incubated in 10% NaOH for 3 d to digest cells, washed three times in 0.1 mol/L Na-perchlorate and two times in deoxygenated, deionized H_2O. The resulting solids were analyzed by XRD. The XRD pattern (not shown) exhibited a relatively high signal-to-noise ratio with broad maxima that was consistent with patterns for fine-grained uraninite. The XRD patterns were identical to those previously reported for biogenic UO_2(s) (Fredrickson et al., 2000).

2.2. Bacterial Reduction Experiments

The ability of *S. putrefaciens* CN32 to reduce U(VI), as uranyl acetate, was evaluated in the presence or absence of pyrolusite, birnessite, bixbyite, and gibbsite ($Al[OH]_3$). Oxide slurries were made to concentration in water and mixed thoroughly while removing aliquots. In a typical experiment with 10 mL final volume, 2.5 mL of 34.8 g L^{-1} pyrolusite slurry were added to replicate pressure tubes, followed by 4.5 mL of 60 mmol/L $NaHCO_3$ buffer, 1.0 to 1.9 mL deionized water, and 0.1 to 1 mL of 10 mmol/L U acetate. Tubes were purged with N_2:CO_2 (80:20) and sealed with thick butyl rubber stoppers. One milliliter of CN32 cell suspension was added from a freshly washed culture of 2 to 4 $\times$ 10^9 cells mL^{-1} in 30 mmol/L $NaHCO_3$ using a needle and syringe purged with N_2:CO_2. Ten milliliters of H_2 were added using a needle and syringe. All experiments were incubated at 30°C with gyratory shaking at 60 rpm. The predominant aqueous U(VI) species was computed to be $UO_2(CO_3)_3^{4-}$(aq) using MINTEQA2 using the best thermodynamic data compiled by the authors.

2.3. Abiotic Experiments With Biogenic UO_2(s) and Mn Oxides

The kinetics of oxidation of biogenic uraninite (UO_2[s]) by the Mn(III/IV) oxides were determined in the absence of bacteria. In a typical experiment with 10 mL final volume, 2.5 mL of 34.8 g L^{-1} pyrolusite slurry were added to replicate pressure tubes, followed by 5 mL of 60 mmol/L $NaHCO_3$ buffer and 1.8 mL deionized water. Tubes were purged with N_2:CO_2 (80:20) and sealed with thick butyl rubber stoppers. Finally, 0.7 mL of a biogenic uraninite suspension ($\sim$360 μmol/L) were added using a needle and syringe.

2.4. Analyses

At selected times, replicate tubes were transferred to an anaerobic (Ar:H_2, 95:5) glove bag (Coy Laboratory Products, Inc., Grass Lake, MI), and 1 mL of suspension was sampled with a syringe and filtered through a 0.2-μm polycarbonate or a 10-K molecular weight cutoff (Pall Filtron Corp., Northborough, MA) filter. This fraction was considered the soluble fraction and analyzed for U(VI) with a kinetic phosphorescence analyzer (Chemchek Instruments, Richland, WA). Mn(II) concentrations were determined by inductively coupled plasma analysis of 0.5 N HCl- or anaerobic 10 mmol/L $CuSO_4$-extracted (20 h) samples. The anaerobic $CuSO_4$ extraction method has been shown to remove $>$90% of the δMnO_2-bound Mn(II) in microbially reduced mineral suspensions (Burdige and Nealson, 1985, 1986). The pH was measured under anaerobic conditions using a Ross combination electrode.

2.5. Transmission Electron Microscopy (TEM)

To eliminate the exposure of reduced mineral solids to oxygen, the whole embedding procedure, as well as the thin sectioning on the microtome, was conducted in an anaerobic glove bag (Ar:H_2, 95:5). Cell-mineral suspensions were gently pelleted by ultracentrifugation, washed in deionized water, and briefly fixed in 2.5% glutaraldehyde. After another wash in anaerobic water, the cell-mineral pellets were gradually dehydrated in ethanol series and infiltrated in LR White embedding resin. Cured blocks were sectioned with a Diatome 35° diamond knife using a Reichert Ultracut E ultramicrotome. Ultrathin sections, 50 to 70 nm, were mounted on copper grids with Formvar support film coated with carbon. To preserve the fragile system redox chemistry, staining with usual heavy metal TEM stains was omitted. To partially compensate for the resulting significant decreases in cell contrast, the smallest objective aperture was used for imaging. Sections were examined at 200 kV using a JEOL 2010 HR transmission electron microscope.

2.6. X-Ray Absorption Measurements (X-Ray Absorption Fine Structure [XAFS])

The manganese X-ray absorption near-edge structure (XANES) and extended X-ray absorption fine structure (EXAFS) spectroscopic studies (XANES and EXAFS are collectively called XAFS) were performed on the hard X-ray microprobe beamline X26A at the National Synchrotron Light Source (NSLS) (Brookhaven National Laboratory, Upton, NY). Microprobe Mn XAFS data were collected using monochromatic light at the Mn K absorption edge (6.539 keV) on the filtered Mn-containing solids after reaction with biogenic UO_2(s), the filtered Mn-containing solids after reaction with abiotic UO_2(s), and the Mn(III/IV)-oxide (pyrolusite, birnessite, and bixbyite) and $MnCO_3$ (rhodochrosite) reference materials at room temperature. Samples were stored under a reducing atmosphere until analyzed. Samples and reference materials were prepared for XAFS analyses by mounting submilligram sample quantities in a square hole cut from a thin plastic sheet that was sandwiched between two layers of Kapton tape. This type of sample containment permitted the collection of transmission-based XAFS data on Mn oxide particles at locations that had thicknesses of a few Mn oxide particles. In particular, these regions were found at the interfaces between the edges of the square-cut holes and the Kapton. Biologically reduced samples were maintained under anoxic conditions until samples were prepared for a specific beam run. The time between when the samples were inoculated and when the XAFS measurements were made varied between experiments but ranged from 4 to 8 weeks.

The micro-XAFS data were collected in transmission mode using a focused X-ray beam and a channel-cut Si(111) monochromator operating at 2.8 GeV with an average current of 200

mA. A highly focused monochromatic X-ray beam at the Mn K edge was obtained using microfocusing optics that consisted of a double-elliptical, Pt-coated Kirkpatrick-Baez mirror system. The mirror system was operated at a pitch of 3 mrad to focus a 350×350 μm^2 monochromatic beam at the Mn K absorption edge down to a 15×15 μm^2 beam (Smith and Rivers, 1995). These optics help reject higher order harmonics and fix the focal spot position in conjunction with a variable-exit, channel-cut monochromator. Typical measurements were made at locations on the sample mount where the transmittance was constant on a spatial scale of 9 times the size of the X-ray beam and absorption path lengths for microanalysis had an absorption edge step of ~1.2 ln units.

Ion chambers were used to collect incident (I_o) and transmission (I_t) signals. Linearity checks of the I_o signal and the I_t signal indicated that the signal was linear to <1% for a 50% reduction in I_o. The sample stage was rotated to 35° to I_o to achieve the magic angle between the surface normal and the plane of polarization of the incoming beam and the sample to eliminate orientation effects of microcrystallites. Mn XAFS data were collected in step sizes of 0.075 $Å^{-1}$, at acquisition times of 28 s, and over an energy range of −170 to +580 eV above the Mn K absorption edge. Spectra were acquired for up to three replicate samples each of the abiotic and biotic samples, and typically, three scans were acquired for each replicate. The EXAFS data were analyzed from –170 to +560 eV above the Mn K edge. The background contribution to the EXAFS spectra was removed using an algorithm (AUTOBK) developed by Newville et al. (1993) that minimizes R-space values in low *k*-space. Each data set was read into the WinXAS analysis package (version 1.3, Ressler, 1998). Replicate scans were coadded to improve S/N. The XANES and the k^3-weighted EXAFS (chi) spectra were compared with spectra from the Mn standards. The chi data were Fourier transformed (FT) to yield R-space or radial distribution function plots. Simulated EXAFS spectra were also generated on the basis of the documented crystallographic properties for U and Mn^{2+} using ab initio–based theory, which involved FEFF 7.2 (Rehr and Albers, 1990; de Leon et al., 1991; Rehr et al., 1991; Stern et al., 1995).

3. RESULTS

3.1. Oxidation of Biogenic UO_2(s) by Mn Oxides

An excess of pyrolusite (50 mmol/L as Mn; 3.92 m^2 L^{-1}) and bixbyite (20 mmol/L as Mn; 84.4 m^2/L) extensively oxidized biogenic uraninite (360 μmol/L; Fig. 2). The rate of oxidation was more rapid with the bixbyite (Fig. 2) because of the greater surface area concentration of its suspension and, possibly, higher Mn(III) content. Both oxides showed an initial (1 to 3 h) rapid oxidation of U(IV) to soluble U(VI), followed by an extended slower rate of oxidation. The pyrolusite quantitatively (364 ± 2 μmol/L U[VI]) oxidized the biogenic uraninite within 7 d (data not shown). The initial pH in this and subsequent experiments was 7.1 and was buffered by the 30 mmol/L bicarbonate. The pH would not be expected to change significantly over the course of the experiments, except in cases in which the Mn oxides were reduced to a large extent.

In a separate experiment, UO_2(s) was equilibrated with varying concentrations of pyrolusite, from 0.44 to 8.8 g L^{-1} β-MnO_2, for 24 h. After this period, aqueous U(VI) and 0.5 N HCl-extractable Mn were measured (Fig. 3). Control experiments revealed that only 95 μmol/L Mn in unreduced pyrolusite was soluble in 0.5 N HCl. The oxidation of UO_2 was clearly promoted by increasing concentrations of Mn(IV) oxide, and the higher amounts of U oxidation corresponded directly to higher concentrations of 0.5 N HCl-extractable Mn. After correcting for the controls, there was good stoichiometric agreement between the oxidation of U(IV) to U(VI) and the reduction of Mn(IV) to Mn(II). The ratio of U(VI) to HCl-extractable Mn was 1.2 and 0.97 for the 4.4 and 8.8 g L^{-1} mmol/L β-MnO_2 suspensions, respectively, as expected for stoichiometric two-electron transfer. The ratio of U(VI) to HCl-extractable Mn was 0.5 for the suspension with 0.44 mg L^{-1} pyrolusite. The reason for the deviation from one at the lower pyrolusite concentration is unclear.

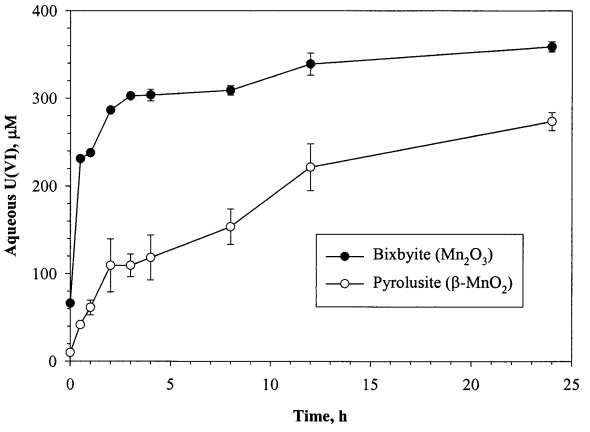

Fig. 2. Oxidation of biogenic uraninite (360 μmol/L) to U(VI) by bixbyite (3.16 g L^{-1}) and pyrolusite (4.35 g L^{-1}) in 30 mmol/L, pH 7.1 HCO_3 buffer.

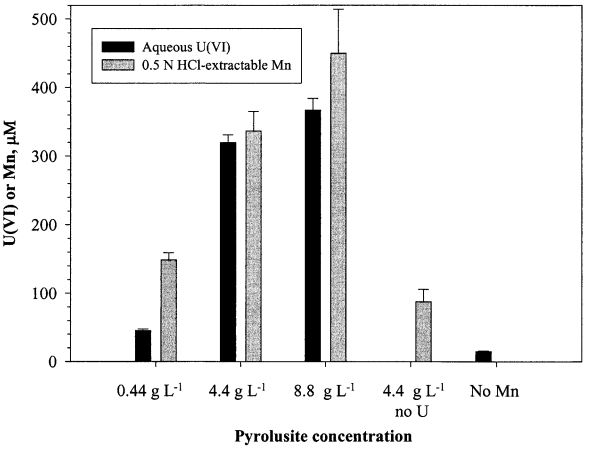

Fig. 3. Oxidation of biogenic uraninite to U(VI) in 30 mmol/L, pH 7.0 HCO_3 buffer by varying concentrations of pyrolusite in suspensions equilibrated for 24 h.

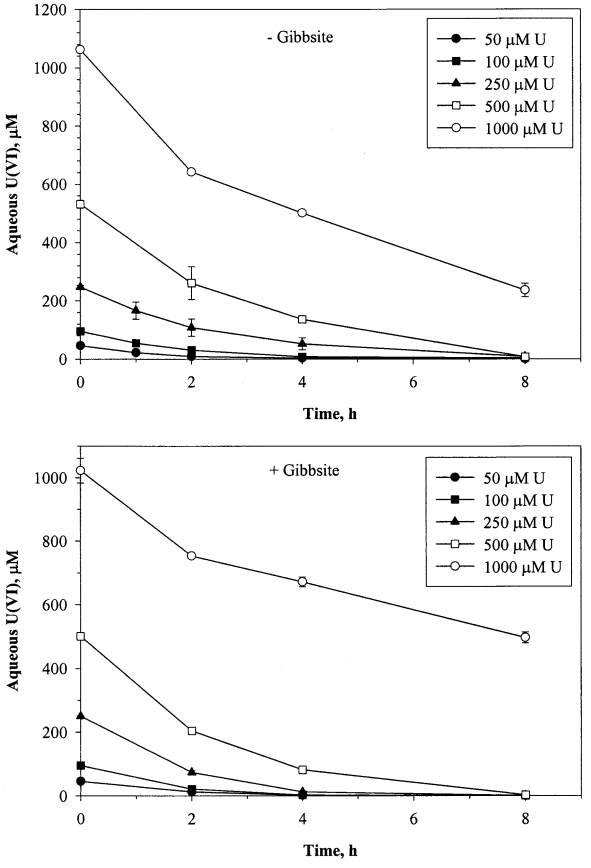

Fig. 4. U(VI) reduction by *Shewanella putrefaciens* strain CN32 in the absence and presence of gibbsite at 1.08 g L^{-1} Al_2O_3 in 30 mmol/L, pH 7.1 HCO_3 buffer. Gibbsite was added at a concentration sufficient to provide an equivalent surface area provided in the pyrolusite experiments. Concentrations of U(VI) listed in the figure legends are the starting values.

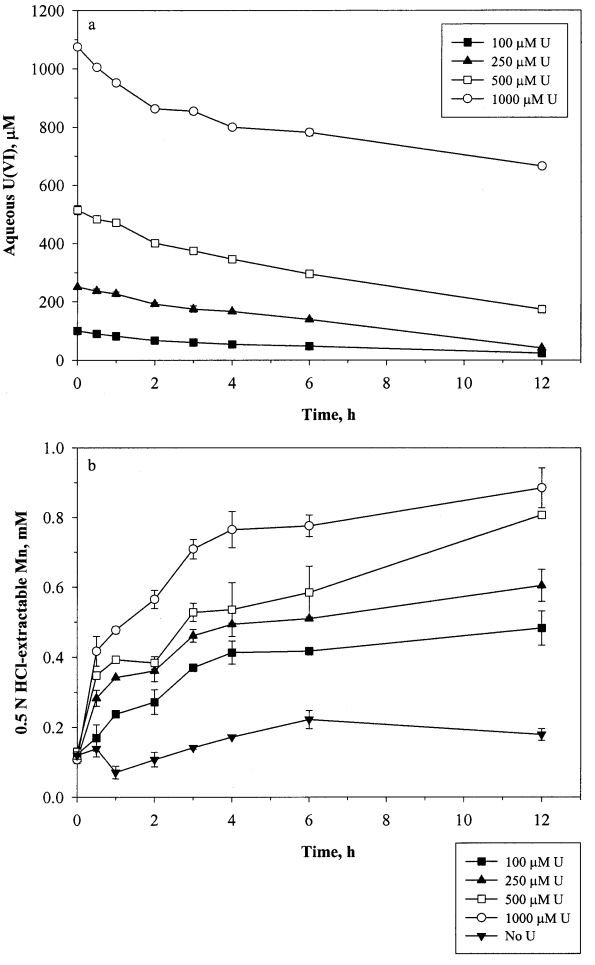

Fig. 5. Reduction of (a) U(VI) and (b) pyrolusite (4.35 g L^{-1}) by *Shewanella putrefaciens* strain CN32 in 30 mmol/L, pH 7.1 HCO_3 buffer. Concentrations of U(VI) listed in the figure legends are the starting values.

3.2. Microbial Reduction of Uranyl Acetate in the Absence and Presence of Gibbsite ($Al[OH]_3$)

The reduction rates of varying concentrations of U(VI) acetate by *S. putrefaciens* CN32 were determined in the absence and presence of gibbsite to establish baselines for assessing the effects of the Mn oxides on the bioreduction process. Gibbsite was used as a non-redox-active phase to determine the effects of mineral surfaces on U(VI) bioreduction. At a concentration of 1.08 g L^{-1}, the total surface area provided by the gibbsite (0.039 m^2/15 mL) was equivalent to that of pyrolusite in the subsequent experiments. Gibbsite does differ in its surface properties from pyrolusite, generally exhibiting a higher positive charge density at the pH of the experiments than pyrolusite. U(VI) was quantitatively removed from solution by bacterial reduction within 8 h at concentrations ranging from 50 to 500 μmol/L (Fig. 4), regardless of whether gibbsite was absent (Fig. 4a) or present (Fig. 4b). In contrast, the rate of U(VI) reduction at 1 mmol/L was slower in the presence of the gibbsite for reasons that are unknown to us at the present time. Nonetheless, U(VI) was quantitatively reduced by CN32 within 24 h in both treatments (later time points not shown). The results of abiotic control experiments conducted under identical conditions but without the bacteria indicated that $<0.5\%$ of the starting U(VI) was removed from solution, except at the highest concentration, 1 mmol/L U(VI), at which abiotic processes such as sorption removed $\sim 7\%$.

3.3. Influence of Mn(III/IV) Oxides on the Bacterial Reduction of U(VI)

In contrast to the gibbsite, pyrolusite at 4.35 g L^{-1} slowed the reduction of U(VI) by CN32 at all U concentrations investigated (Fig. 5a). With the exception of the highest U(VI) concentration (1 mmol/L), $>95\%$ of the initial U(VI) in the gibbsite (−) or gibbsite (+) experiments had been reduced after 4 h, and the U(VI)(aq) concentrations were below detection after 8 h (Fig. 4). In the pyrolusite suspensions, only 26 to 46% of the initial U(VI) at the various concentrations examined had been reduced within 4 h. Even after 12 h, between 16 and 62% of the initial U(VI) remained in solution for the various treatments. Although the sorption of U(VI) to pyrolusite was not investigated directly, in similar experiments with pyrolusite

Table 1. Soluble U(VI) and Mn(II) after long-term (21 d) incubation of Mn oxides and U(VI) with *Shewanella putrefaciens* strain CN32.

	Pyrolusite (4.35 g L^{-1})		Birnessite (1.74 g L^{-1})		Bixbyite (3.16 g L^{-1})	
U(VI) (μmol/L)	U(VI) (μmol/L)	Mn[a] (μmol/L)	U(VI) (μmol/L)	Mn[b] (μmol/L)	U(VI) (μmol/L)	Mn[c] (μmol/L)
1000	0	3352	428	402	148	7560
500	0	1712	23	238	2	4967
0		805[d]		176		2259
No cells, 0		94		15		1409

[a] 0.5 N HCl extractable.
[b] 10 mmol/L, pH 4.7 $CuSO_4$ extractable.
[c] 0.5 N HNO_3 extractable.
[d] Mn analysis from 50 h, rather than 21 d, incubation.

(4.35 g L^{-1}) and 250 μmol/L U(VI) in 30 mmol/L, pH 7.1 bicarbonate buffer with 25 mmol/L Na lactate as the electron donor, the loss of U(VI) from solution attributable to abiotic processes such as sorption was <4%.

Concurrent with the slower rates of U(VI) reduction were increases in the concentration of 0.5 N HCl-extractable Mn. Increasing initial concentrations of U(VI) corresponded directly to increasing concentrations of HCl-extractable Mn with time (Fig. 5b). Relatively little pyrolusite was reduced in the absence of U(VI) over the first 12 h of the experiment. Analyses following extended (21 d) incubation revealed that the U(VI) concentration had decreased to below detection in both the 500-μmol/L and 1-mmol/L U(VI) treatments and that the HCl-extractable Mn concentrations had increased significantly, to 1.7 and 3.4 mmol/L, respectively, for these same U concentrations (Table 1).

To determine the generality of the pyrolusite results and to qualitatively address the effects of valence, structural, and surface properties of the Mn oxides on bacterial U(VI) reduction, experiments were conducted with birnessite ($K_4Mn_{14}O_{27} \cdot 8H_2O$) and bixbyite ($Mn_2O_3$) with U(VI) at 500 μmol/L and 1 mmol/L. Similar to the experiment with pyrolusite, both birnessite and bixbyite (Fig. 6a) inhibited the reduction of U(VI) by CN32, and U(VI) enhanced the reduction of Mn, as determined by increases in the $CuSO_4$-extractable Mn fraction with time (Fig. 6b). The concentrations of $CuSO_4$-extractable Mn were higher for the bixbyite than the birnessite for all treatments, including the control that lacked U(VI), despite the common surface area of the two suspensions (i.e., 84 m^2 L^{-1}). The rates of U(VI) reduction, however, were virtually identical in both the birnessite and bixbyite suspensions for both concentrations of U(VI) studied. Birnessite and bixbyite retarded the bioreduction of U(VI) more than did pyrolusite. In contrast to pyrolusite, some soluble U(VI) remained in solution even after long-term (21 d) incubation with both the birnessite and bixbyite (Table 1). As an illustration of the stability of the pH in the bicarbonate buffer used in these experiments, the pH increased only modestly from 7.1 to 7.4 in the bixbyite suspension with 1 mmol/L U(VI).

An experiment was also conducted with biogenic Mn(IV) oxide from the oxidation of Mn(II) by *Bacillus* sp. strain SG-1 (Nealson and Ford, 1980). This oxide is predominantly Mn(IV), probably vernadite (δ-MnO_2) or one with a similar Mn(IV) local structure (e.g., birnessite; Bargar et al., 2000). Vernadite is a hydrous, slightly crystalline material exhibiting two diffraction lines that are dissimilar to birnessite. A kinetic experiment was performed with the biogenic oxide like those reported in Fig. 6 with an initial concentration of 500 μmol/L U(VI) and biogenic MnO_2 at 1.04 g L^{-1}. After 7 d, 248 ($\pm$3.2) μmol/L U(VI) remained in solution, and the soluble Mn concentration increased from 41 μmol/L at the time of cell inoculation to 301 μmol/L after 7 d. Thus, the biogenic MnO_2 was equally or more reactive with U(IV) than were the synthetic Mn

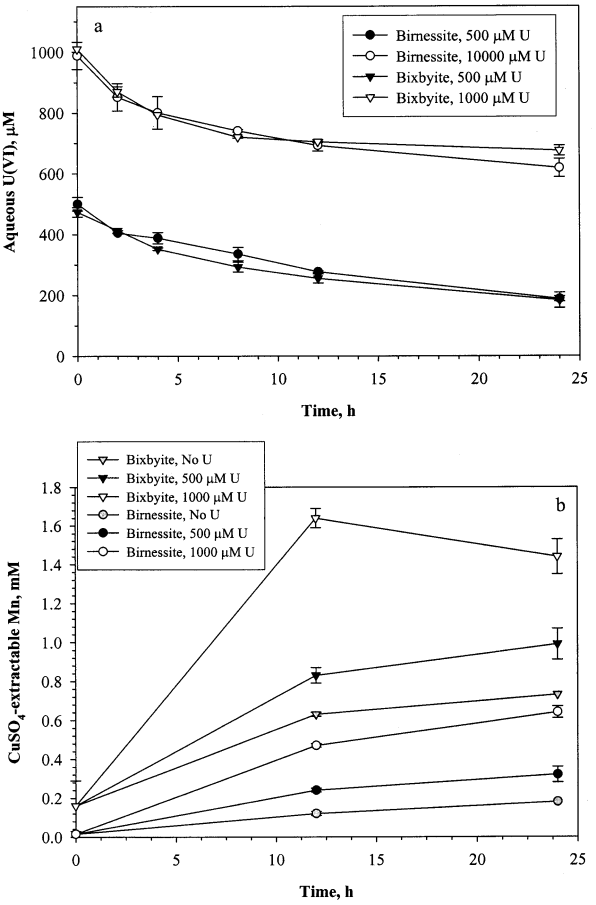

Fig. 6. Reduction of U(VI) (a) in the presence of birnessite (1.74 g L^{-1}) and bixbyite (3.16 g L^{-1}) by *Shewanella putrefaciens* strain CN32 in 30 mmol/L, pH 7.1 HCO_3 buffer. Mn(II) (b) was determined by extraction with 20 mmol/L, pH 3.7 $CuSO_4$. Concentrations of U(VI) listed in the figure legends are the starting values.

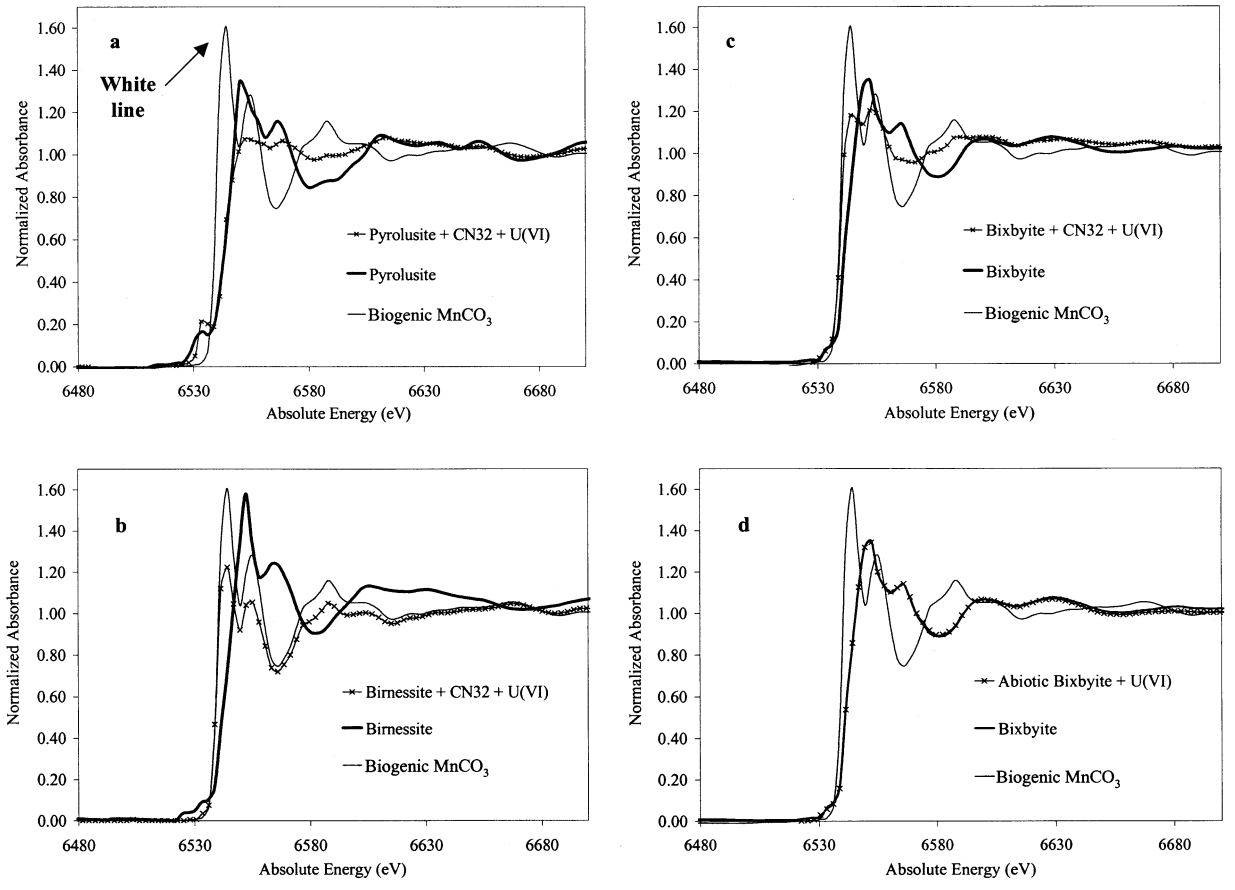

Fig. 7. Mn X-ray absorption near-edge structure spectra of bioreduced Mn oxides and U(VI) relative to unreduced pyrolusite and rhodochrosite standards: (a) pyrolusite, (b) birnessite, (c) bixbyite, and (d) bixbyite abiotic (no cells) control.

oxides (Table 1), although the surface area was not measured, complicating direct comparisons.

Mn XANES analyses provide information on oxidation state and some information about the local structural environment of the Mn in our sample. The Mn XANES analyses of solids from the pyrolusite suspensions incubated with CN32 and 500 μmol/L U(VI)-acetate revealed spectra that were similar to unreduced pyrolusite (Fig. 7a), although the white line and other postedge features in the XANES spectra for this treatment were decreased relative to that of the pyrolusite standard. This similarity to unreduced pyrolusite was consistent with the relatively small amount of HCl-extractable Mn (<2%) that was measured in these samples (Fig. 5b). In contrast, bioreduced suspensions containing birnessite or bixbyite gave rise to spectra (Figs. 7b and 7c, respectively) that were similar to biogenic rhodochrosite ($MnCO_3$). However, the postedge spectral features in the XANES spectra for these two treatments were less pronounced than that of the biogenic $MnCO_3$. Rhodochrosite is a kinetically viable Mn(II) precipitate in bicarbonate buffer (Johnson, 1982). It is also the thermodynamically stable phase in our experiments at the final pe and pH values at the given Mn(II) and carbonate concentrations. In the abiotic experiment in which UO_2(s) was allowed to react with an excess of bixbyite (Fig. 2), the Mn XANES spectra were nearly identical to that for unreacted bixbyite (Fig. 7d).

The Mn EXAFS analyses provide additional speciation information about the Mn solids in the samples after treatment. Specifically, the Mn EXAFS data provide highly detailed atom-scale information on the local structural environment of the Mn in our samples. The k^3-weighted Mn EXAFS data for the biotic pyrolusite treatment (Fig. 8a) show some similarities to those of the pyrolusite standard and the simulated pyrolusite spectra, but the amplitudes of the oscillations are small relative to the pyrolusite standard and simulation. Linear combinations of pyrolusite and biogenic $MnCO_3$ spectra did not adequately simulate these spectra. Linear combinations were not performed with the chi data for the bioreduced birnessite, because the spectra had a strong similarity to that of $MnCO_3$ (Fig. 8b). The chi data for the bioreduced bixbyite treatments (Fig. 8c) could be simulated with a roughly 50:50 combination of the $MnCO_3$ and bixbyite spectra, but only up to chi values of $\sim$8 $Å^{-1}$ (linear combination data not shown). In contrast to this biotic bixbyite treatment, the chi data for the abiotic control with bixbyite (Fig. 8d) indicate that the bixbyite did not undergo changes in Mn speciation.

The FT data for the biotic pyrolusite sample indicate that it is rich in pyrolusite and contains little $MnCO_3$ (compare Fig. 9a with $MnCO_3$ spectra in Fig. 9b). The FT data for the biotic bixbyite sample indicate that there is considerable destructive interference, but peaks from bixbyite and $MnCO_3$ phases dom-

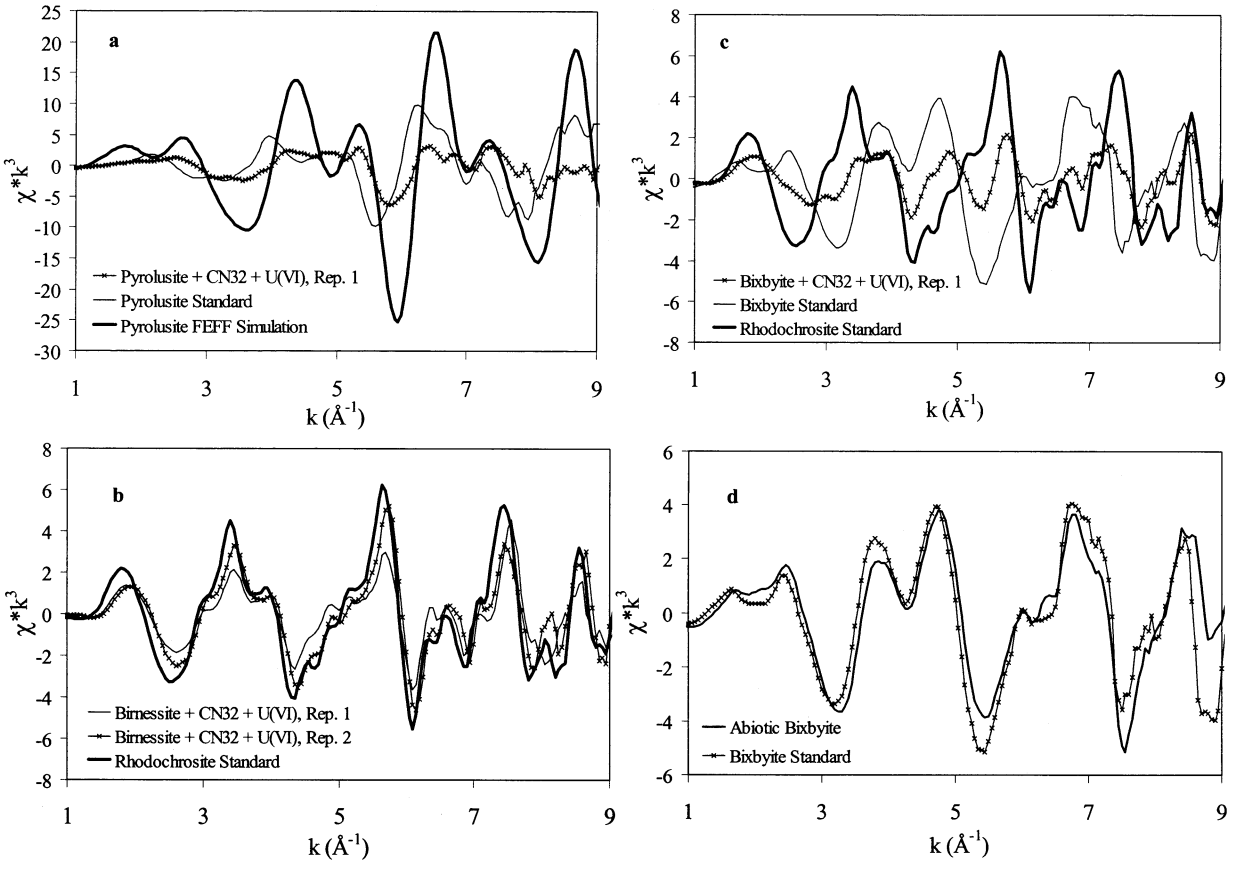

Fig. 8. Mn k^3-weighted chi spectra of bioreduced Mn oxides and U(VI) relative to unreduced pyrolusite and rhodochrosite standards: (a) pyrolusite, (b) birnessite, (c) bixbyite, and (d) bixbyite abiotic (no cells) control.

inate the spectra (Fig. 9b). The FT data for the biotic birnessite treatment show almost complete conversion to $MnCO_3$ (Fig. 9c). The FT data for the abiotic bixbyite treatment (not shown) showed that the control did not undergo transformation to another phase during the experiment. We did have initial concern that bixbyite might transform to a more stable Mn(III/IV) phase. Collectively, the results of the EXAFS analyses demonstrated that the pyrolusite treatments were more resistant to bioreduction than were bixbyite or birnessite and that in the absence of microbial reduction, the bixbyite did not change to other oxide phases during incubation.

3.4. TEM Analyses of U Localization in Cell and Cell-Mn Oxide Suspensions

In the absence of Mn(III/IV) oxide, thin sections of fixed and embedded cell suspensions indicated that the U(IV) was present as fine-grained precipitates external to the cell, as well as in association with cell walls (Figs. 10a and 10b). This fine-grained biogenic U(IV) precipitate was previously demonstrated to be uraninite (UO_2[s]) by XRD and XANES (Fredrickson et al., 2000). There was no evidence among the images examined to suggest that some cells had lysed, possibly accounting for the extracellular UO_2(s).

In the CN32 cell suspensions incubated with U(VI) and birnessite, in which the rate of U(VI) reduction was impeded (Fig. 6), the distribution of U(IV) was quite different from those incubated without the Mn(III/IV) oxides. Most notable was the absence of fine-grained extracellular U(IV) precipitate and the presence of U(IV) exclusively in association with cells in the suspensions with bixbyite (Fig. 10c) or birnessite (Fig. 10d). Consistent with the Mn XANES and EXAFS analyses, rhombohedral rhodochrosite particles were observed in the bioreduced suspension of bixbyite (Fig. 10c).

Higher resolution images of cells in the bixbyite suspensions revealed a heavy accumulation of U(IV) in the periplasm of the cells (Figs. 10e and 10f). The composition of these phases was predominantly U and lacked any detectable Mn, as determined by energy-dispersive spectroscopy (EDS). The extracellular crystallites in Figures 10c and 10d were Mn oxide particles that did not contain detectable levels of U, as determined by EDS. High-resolution TEM revealed the fine-grained nature of the periplasmic material that yielded lattice fringe images with d-spacings consistent with uraninite (not shown).

4. DISCUSSION

4.1. Bioreduction of U(VI)

Suspensions of the subsurface bacterium *S. putrefaciens* CN32 quantitatively reduce aqueous U(VI) (50 μmol/L to 1 mmol/L) in pH 7 HCO_3^- buffer to insoluble (0.2 μm–filter-

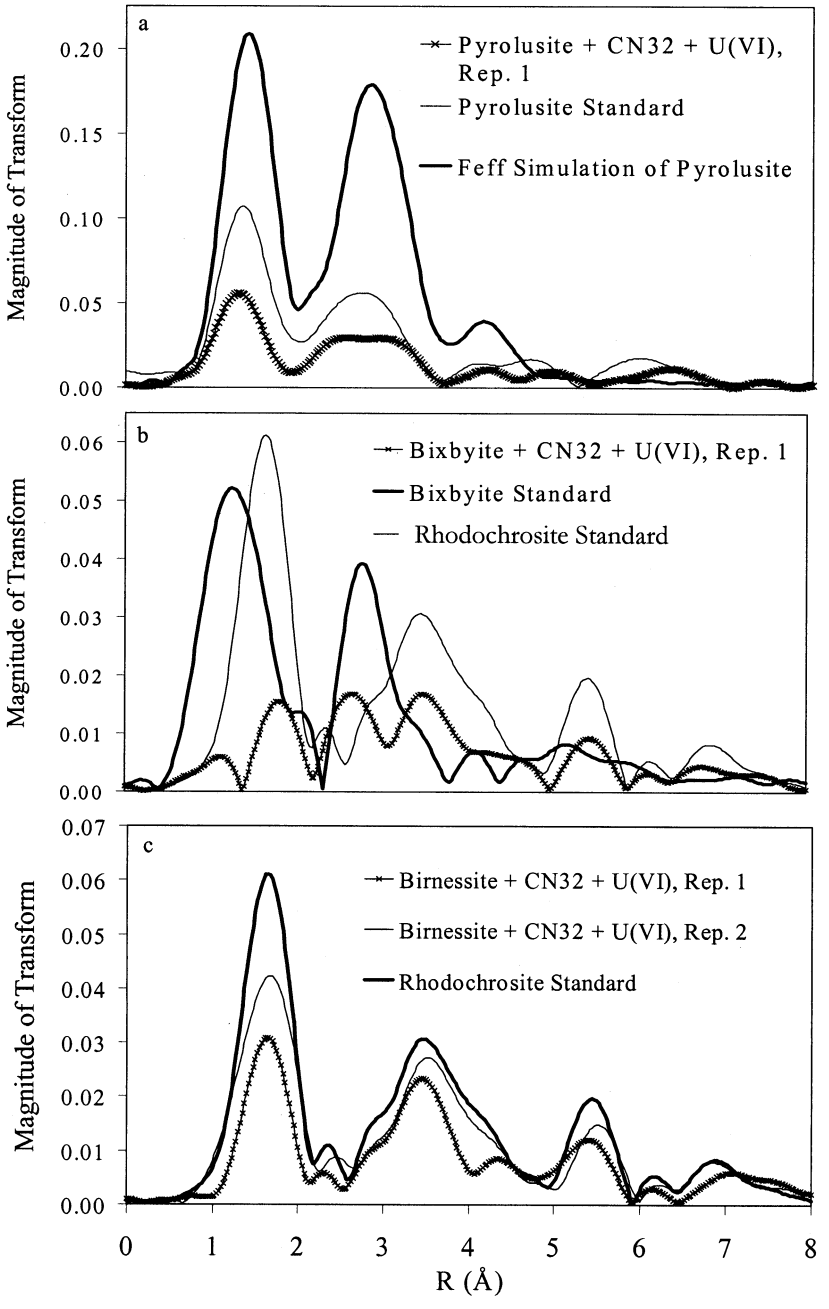

Fig. 9. Fourier-transformed Mn X-ray absorption fine structure spectra of bioreduced Mn oxides and U(VI) relative to unreduced pyrolusite, FEFF simulations for pyrolusite, unreduced bixbyite, and biogenic rhodochrosite standards: (a) pyrolusite, (b) birnessite, and (c) bixbyite and birnessite (abiotic bixbyite control spectra not shown). All spectra are uncorrected for phase shift.

able) species in <24 h when provided excess H_2 as an electron donor (Liu et al., 2002). The rates of U(VI) reduction in the absence of solids conform to Michaelis-Menten kinetics with K_s = 350 μmol/L and V_m = 200 μmol/L h^{-1} (Liu et al., 2002). Analyses of bulk bioreduced U by XRD and XANES reveal that the product is predominantly UO_{2+x} (uraninite), where x is <0.1 (Fredrickson et al., 2000). The biogenic uraninite is fine grained, with a nominal particle size of 10 nm or less. It exists as an extracellular precipitate and in the periplasmic space (Figs. 10a and 10b). In experiments investigating the reduction of TcO_4^- by CN32 or *Geobacter sulfurreducens*, similar distributions of reduced Tc, probably as TcO_2, were observed in cell suspensions incubated with H_2 as the electron donor (Wildung et al., 2000).

The above-noted distribution of biogenic UO_{2+x} is consistent with the current understanding of electron transfer mechanisms in metal-reducing bacteria that indicate that metal-reductase activity is associated with the cell membrane,

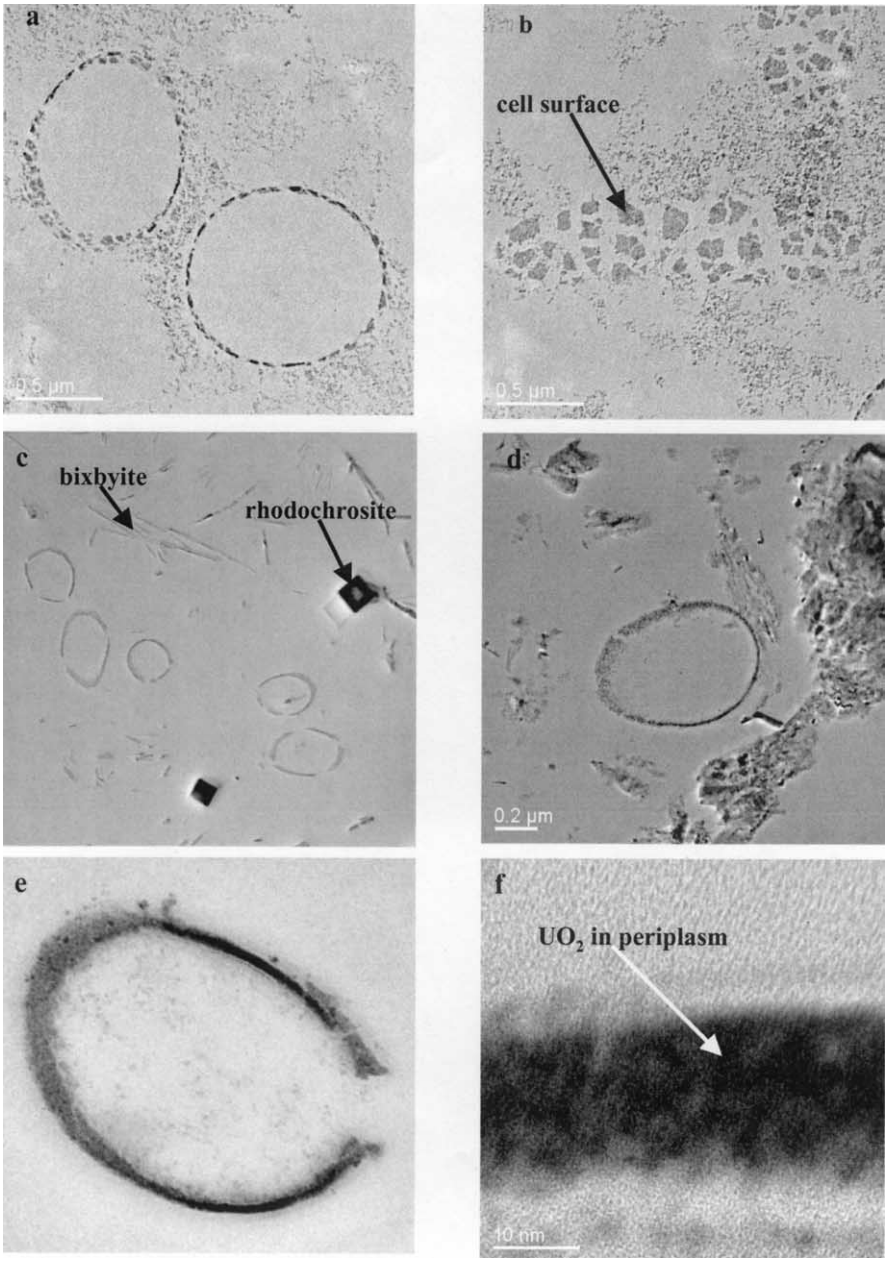

Fig. 10. Transmission electron microscopy images of unstained thin sections from *Shewanella putrefaciens* strain CN32 cells incubated with H_2 and U(VI) in bicarbonate buffer in the absence of Mn oxides, illustrating the accumulation of U(IV) extracellularly and in association with the periplasmic space (a) and cell surface (b). CN32 incubated with H_2 and U(VI) in the presence of bixbyite or birnessite exhibited an absence of fine-grained extracellular UO_2(s) and accumulation of UO_2(s) almost exclusively in the periplasm (e and f).

periplasmic space, and OM. Under anaerobic conditions, metal-reducing bacteria link proton translocation to metal respiration, a process that yields sufficient energy for ATP synthesis. In most Gram-negative bacteria, respiratory cytochromes reside in the cell or inner membrane and in the periplasmic space. However, in *S. oneidensis* MR-1, ferric reductase activity is also associated with the OM (Beliaev and Saffarini, 1998). OM cytochromes have been repeatedly isolated from *Shewanella* strains that were cultured anaerobically (Myers and Myers, 1988, 1992, 1997). An OM *c*-type cytochrome, omcA, was released by *Shewanella frigidimarina* into solution during incubation, suggesting that this cytochrome was associated with the exterior face of the OM and may function as a terminal reductase during Fe(III) reduction (Field et al., 2000). In *G. sulfurreducens*, ferric reductase activity is associated with OM fractions (Magnuson et al., 2000), possibly the outside of the OM (Gaspard et al., 1998). Outward-facing OM-associated cytochromes may facilitate the transfer of electrons from the electron transport system of the bacteria to surface functional groups on the surfaces of insoluble Fe(III) and Mn(III/IV).

Table 2. Reduction potentials of the Mn(III/IV) oxides, uranyl carbonate, and Fe(III) oxides.

	Eh°(v)	Eh'(v)
Birnessite (MnO_2)[a,b,c]		
$1/2MnO_2 + 1.5H^+ + e^- + 1/2HCO_3^- = 1/2MnCO_3 + H_2O$	1.30	0.620
Pyrolusite (MnO_2)[b,c]		
$1/2MnO_2 + 1.5H^+ + e^- + 1/2HCO_3^- = 1/2MnCO_3 + H_2O$	1.23	0.558
Bixbyite (Mn_2O_3)[b,c]		
$1/2Mn_2O_3 + e^- + 2H^+ + HCO_3^- = MnCO_3 + 3/2H_2O$	1.50	0.557
Aqueous uranyl carbonate[d]		
$0.5UO_2(CO_3)_3^{4-}(aq) + 1.5H^+ + e^- = 0.5UO_2(s) + 1.5HCO_3^-$	0.687	0.078
Ferrihydrite ($Fe[OH]_3$)[a,e,g]		
$Fe(OH)_3 + 2H^+ + e^- + HCO_3^- = FeCO_3 + 3H_2O$	0.971	0.0250 (0.0529)[e]
Goethite (α-FeOOH)[e,g]		
α-FeOOH + $2H^+ + e^- + HCO_3^- = FeCO_3 + 2H_2O$	0.848	–0.0983

[a] Assumed stoichiometry for ease of computation.
[b] In equilibrium with $MnCO_3$, pH = 7, and $HCO_3^- = 10^{-2}$ mol L^{-1}.
[c] Thermodynamic data from Robie et al. (1979).
[d] Computed stable U(VI) aqueous species in 30 mmol/L $NaHCO_3$ buffer.
[e] In equilibrium with $FeCO_3$, pH = 7, and $HCO_3^- = 10^{-2}$ mol L^{-1}.
[f] Eh° for 30 mmol/L HCO_3^- as used by Wielinga et al. (2000).
[g] Thermodynamic data from Lindsay (1979).

Electron-accepting metals, such as U(VI) or Tc(VII), are soluble in their most oxidized form and are free to engage with electron transfer proteins, whether they are localized in the periplasm or the OM. Because of their low solubility, U(IV) or Tc(IV) probably precipitate at or near the site of reduction. However, the rate of UO_2(s) precipitation relative to the rate of microbial U(VI) reduction is not known. In experiments with *Geobacter metallireducens*, U(IV) produced as a result of bacterial reduction passed through a 0.2-μm filter during the early stages (~7 h) of reduction, but thereafter was completely filterable (Gorby and Lovley, 1992). These results suggest that UO_2(s) precipitation kinetics may be slower than bacterial reduction or that the initial precipitates are colloidal (<0.2 μm). Whether the <0.2-μm U(IV) is an aqueous species or a colloidal phase is unknown, but the observations suggest the production of an initially mobile U(IV) species that may diffuse from the periplasm or cell surface to the bulk medium before precipitation and aggregation into larger crystallites.

4.2. Abiotic Reactions

In the absence of microbiological activity, bixbyite and pyrolusite oxidized biogenic UO_2(s) to soluble U(VI) species in bicarbonate buffer in suspensions that were constantly mixed (Fig. 1). These experimental results are consistent with the reduction potentials of U(VI) and the Mn(III/IV) oxides (Table 2). The thermodynamic data of Robie et al. (1978) indicate that birnessite is the strongest oxidant under the experimental conditions (e.g., Eh at pH 7), followed by bixbyite and pyrolusite, which exhibit nearly identical s values. Additional calculations using the half-cell potentials for pyrolusite and the U(VI)-U(IV) system and solubility products for MnO_2(s), $MnCO_3$(s), and UO_2(s) underscore the strong oxidizing potential of Mn(IV) and indicate that 5 log units in pe separate the stability region of UO_2(s) and MnO_2(s) (Fig. 11). None of the Mn(III/IV) oxides can coexist with UO_2(s) at equilibrium.

The computed concentration of U(IV)(aq) (log [C] $\leq 10^{-10}$ mol L^{-1}; Fig. 11) highlights the low solubility of UO_2(s) and the potential effectiveness of U(VI) bioreduction as a remedial strategy. Even though pyrolusite has a higher oxidation potential, bixbyite was more reactive with the biogenic UO_2(s). We surmise that this was at least in part a surface area effect. The total surface area concentration of the bixbyite suspension (84.4 m^2 L^{-1}) was more than 20-fold greater than the pyrolusite suspension (3.9 m^2 L^{-1}). Other factors, however, may also have been at play, such as differences in (a) surface site densities of reactive functional groups, as controlled by crystallite structure, morphology, and defect density; (b) interfacial electron transfer rates; or (c) Mn oxidation state. Also, there is evidence to suggest that Mn(III) centers may be involved in the oxidation of Cr(III) to Cr(VI) by birnessite (Nico and Zasoski, 2000). If true, this could explain in part why the bixbyite was especially reactive with the biogenic UO_2(s).

While the reduction potentials of U(IV)/U(VI) indicate that the Mn(III/IV) oxides should be effective oxidants of U(IV), the fact that both the Mn oxides and biogenic UO_2(s) are poorly soluble at circumneutral pH provided uncertainty as to whether these reactions would proceed and to what extent. The electron transfer process probably involved grain-to-grain contact and coordinative interactions between surface functional groups on the two dissimilar solid phases. Surface contact between the two solid phases was facilitated in our experiments by continuous shaking. The high surface area and small particle size (~10 nm) of the biogenic UO_2(s) may have allowed its collection (e.g., sorption) by the larger Mn(III/IV) oxide particles. The 2.6×10^{-2} mol L^{-1} bicarbonate buffer enhanced the release of U(VI) from the UO_2(s) surface and minimized surface passivation through the formation of aqueous U(VI)-carbonate complexes.

The extent to which these complex interparticle electron transfer reactions may occur in situ will depend on the form and physical distribution of U(IV) and the spatial locations of metal-reducing bacteria in relation to the Mn oxides. In soils and sediments, Mn(III/IV) oxides occur as immobile coatings or microparticulate precipitates on larger grain surfaces, as

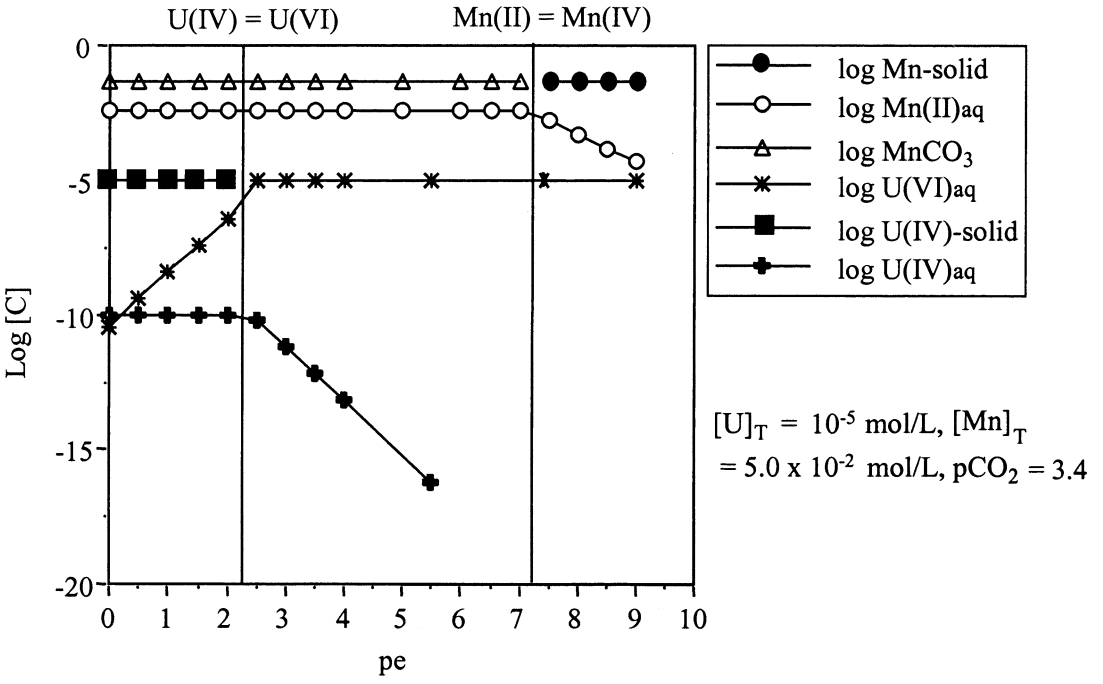

Fig. 11. Computed equilibrium valence speciation of U and Mn at pH 7 as a function of overall redox potential (pe).

interparticle cements (Zachara et al., 1995), and as deposits in fractures and veins (McKenzie, 1989). Their capacity to function as oxidants for organic and inorganic ions is dependent on their exposed surface area; the properties of the exposed surfaces, such as charge type and distribution; and physical contact that allows electron transfer through coordinative interaction. While soluble species are more likely to come in contact with Mn(III/IV) oxides through water advection or diffusion, colloids of sparingly soluble reduced metals and radionuclides (e.g., U, Tc, and Pu) can also be mobile (McCarthy and Zachara, 1989) and able to physically contact oxidizing mineral surfaces. It is not currently known whether biogenic UO_2(s) has potential for dispersion and colloid migration in subsurface systems. Clearly, it will be important to more thoroughly investigate the speciation and fate of U(IV), particularly during the early phases of bacterial reduction, to better predict U fate during in situ bioreduction.

Microbial reduction of Mn(IV) could potentially contribute to the oxidation of solid-phase U(IV) by forming soluble Mn(III) complexes as intermediates in the reduction of Mn(IV) oxides (Ehrlich, 1987). These complexes could subsequently react with U(IV). Although Mn(III) is generally present as a discrete (e.g., MnOOH) or mixed solid phases with Mn(IV) (e.g., bixbyite), aqueous Mn(III) complexes with strong ligands may be present in soil extracts and in aquatic environments (Luther et al., 1994). Aqueous complexes such as Mn(III)-pyrophosphate may be important environmental oxidants, even if short lived (Kostka et al., 1995).

4.3. Mn Oxide Impact on U Bioreduction

Mn(III/IV) oxides may affect microbial U(VI) reduction by several mechanisms. One mechanism is the oxidation of biogenic UO_2(s) by Mn(III/IV), as discussed above. Another mechanism is by competition for liberated electron equivalents. Both Mn(III) (Kostka et al., 1995) and Mn(IV) (Nealson and Saffarini, 1994) can serve as terminal electron acceptors for *S. putrefaciens* during anaerobic respiration. Although Mn(III) and Mn(IV) are thermodynamically favored (i.e., the potential energy gain is higher) as electron acceptors relative to U(VI) (Table 2), the oxidized forms of Mn are poorly soluble at circumneutral pH. Hence, the bioavailability of Mn(III/IV) may be significantly lower than soluble U(VI) complexes.

Insights into the relative bioavailability of the various Mn(III/IV) oxides used in the studies reported herein can be gained by examining the extent of their reduction in the absence of U (Figs. 5 and 6). Pyrolusite was poorly reducible in the absence of U(VI): The concentration of 0.5 N HCl-extractable Mn following incubation for 50 h that could be attributed to bioreduction was 711 μmol/L. Birnessite was also poorly available: Only 161 μmol/L $CuSO_4$-extractable Mn were produced after 21 d, while bixbyite was the most reducible of the three oxides at 850 μmol/L. The greater reducibility of bixbyite was not expected on the basis of thermodynamic properties (Table 2). The differences in the bioreducibility of the three oxides may therefore be attributed to other factors such as suspension surface area (e.g., 3.92 $m^2\ L^{-1}$ for pyrolusite vs. 84.4 $m^2\ L^{-1}$ for bixbyite and birnessite), crystal structure, and structural disorder. Of these, the latter two factors appear most significant. Pyrolusite is the most ordered phase of the three oxides studied, and exhibits a stable tetragonal rutile structure with corner-sharing Mn octahedra. Birnessites, in contrast, are poorly ordered phyllomanganates with edge-sharing Mn octahedra with large structural and stoichiometric variations (Potter and Rossman, 1979; Souff and Boulegue, 1988; McKenzie,

1989). Little has been published on the structure of bixbyite, but our XRD patterns (Fig. 1) indicated that the phase was significantly disordered. Despite differences in medium, oxide concentration and properties, and organism type, our results were in good agreement with those of Burdige et al. (1992), who found a similar range in concentrations of Mn(II) resulting from the reduction of pyrolusite and birnessite by *S. putrefaciens* MR-1 after incubation for 10 d. Our studies and those of Burdige et al. (1992), however, indicate that the mineralogic and surface chemical factors controlling the bioreduction of different Mn oxides are not well understood. In addition, investigations are required to determine whether naturally occurring Mn oxides may be more susceptible to microbial reduction than their synthetic counterparts, as has been observed for some crystalline Fe(III) oxides (Zachara et al., 1998).

As shown in Figures 5 to 7, we observed that birnessite and bixbyite (at 84 $m^2\ L^{-1}$) affected U(VI) reduction to an identical extent, while pyrolusite (at 3.4 $m^2\ L^{-1}$) allowed more rapid U(VI) bioreduction. These results implied that the total surface area of the Mn(III/IV) oxide phase, rather than its structure or thermodynamic/surface properties, was the most important factor controlling the impact on U(VI) bioreduction. We concluded, therefore, that U(IV) oxidation by the Mn(III/IV) oxide surface, rather than electron acceptor competition, was the primary causal mechanism for the retardation of U(VI) bioreduction. Hence, the rate of biologic U(VI) reduction may have been similar in the presence and absence of Mn oxides, but the net rate of reduction was significantly lower because of the oxidation of U(IV) by the oxides.

The reduction of Mn increased with increasing U(VI) concentration regardless of Mn oxide type, suggesting that U(IV) was facilitating electron transfer from the bacterial cells to the oxide surfaces. Although the specific mechanisms remain unclear, the results indicate that U(IV) was functioning as an electron shuttle, similar to the manner in which humic acids, AQDS, and other quinone-containing organic compounds promote the rate and extent of reduction of Fe(III) oxides (Lovley et al., 1998; Zachara et al., 1998). Quinones can serve as electron acceptors for DMRB (Lovley et al., 1996) and in the process are reduced to hydroquinones (Scott et al., 1998) that function as facile reductants of Fe(III) oxides (Kung and McBride, 1988b) and Mn(III/IV) (Stone and Morgan, 1984; Kung and McBride, 1988a). In contrast to the water-soluble quinones, the solubility of U(IV) is low (Fig. 11), and as a result, the U(IV) pool increases with incubation time because some portion of the biogenic precipitate is no longer available to react with the Mn oxides. In the case of pyrolusite, no soluble U(VI) was present in suspensions with 0.5 or 1 mmol/L initial U(VI) after 21 d of incubation, despite an excess of Mn(IV). These suspensions are in thermodynamic disequilibrium with respect to Mn(IV) oxide and UO_2(s) (Fig. 11).

Mechanistic insights into the disequilibrium are afforded by the TEM images of sectioned bacteria-mineral suspensions (Fig. 10). In the absence of Mn oxide, UO_2(s) is present extracellularly, in association with the cell surface, and within the periplasmic space of the cells. In contrast, UO_2(s) in cell suspensions with Mn oxide was exclusively localized within the periplasmic space. UO_2(s) accumulation within the cell periplasm provides direct evidence for the physical separation of UO_2(s) and the Mn oxide particles. A conceptual model for these observations includes the oxidation of extracellular UO_2(s) by the Mn oxides to U(VI), resulting in the formation of soluble U(VI) carbonate species that are free to diffuse into the periplasm, where they are subject, again, to enzymatic reduction. This process can continue until all of the U is precipitated as UO_2(s) within the periplasm, the electron donor is exhausted, the cells become nonviable, or the surfaces of the Mn oxides are no longer reactive.

The high density of UO_2(s) within the cell (Figs. 10e and 10f) is quite remarkable and indicates that the bacteria have a high tolerance for this mineral in their periplasm; they can sustain enzymatic activity in spite of massive UO_2(s) accumulation. The maximum U accumulation before enzymatic activity ceases in the periplasm and cells become nonviable is unknown; the viability of the cells in our suspensions was not determined. Small solutes typically enter the periplasmic space of Gram-negative bacteria via diffusion through porins in the OM that typically have diameters in the range of 1 nm (Nikaido, 1992). These porins likely restrict the movement of UO_2(s) from the periplasm to outside the cell, although the relatively small particle size ($<$10 nm) and slow precipitation and aggregation relative to reduction (Gorby and Lovley, 1992) may allow some export. There is currently little information available regarding the transport of solids through porins. Whether the extracellular UO_2(s) observed in the absence of Mn oxide is derived from U(VI) reduced external to the cells by OM-associated cytochromes or biogenic water soluble quinones or is exported from the periplasm before precipitation or aggregation is currently unknown.

Mn oxides have a significant capacity for sorption of Mn(II) (Morgan and Stumm, 1964), a reaction that occurs rapidly ($<$1 s) at pH 5 (Fendorf et al., 1993). It is not known whether the sorption of Mn(II) influenced the rate and extent of U(IV) oxidation in this study; however, the circumneutral pH of our experiments was conducive to Mn(II) sorption (Stone and Ulrich, 1989). Mn(II) sorption has potential to passivate the oxide surfaces against further redox reactions by complexing with reactive sites on the oxide surface and altering surface charge characteristics. The oxidation of Cr(III), added as $Cr(NO_3)_3$, by birnessite was not affected by presorption of Mn(II) at either pH 3 or 5 (Fendorf et al., 1993), possibly because of relatively low sorption of Mn(II) to the Mn oxide surface compared to Cr(III). While Mn oxides can facilitate the oxidation of Cr(III), the extent of the reaction is a complex function of Cr concentration, solubility, pH, surface area, and ionic strength (Fendorf and Zasoski, 1992). Although surface poisoning by Mn(II) was not a factor in the catalytic activity of pyrolusite toward oxidation of Co(II)$EDTA^{2-}$, an intermediate Mn(III) oxide surface complex appeared to slow the oxidation rate (Jardine and Taylor, 1995). It is also possible that Mn oxide surfaces could be physically blocked from interacting with U(IV) by surface precipitation of $MnCO_3$(s), although the TEM images indicate that rhodochrosite was present as distinct crystallites in the oxide-bacteria suspensions (Fig. 10c).

5. IMPLICATIONS TO IN SITU U BIOIMMOBILIZATION

Mn(III/IV) oxides were shown to rapidly and extensively oxidize biogenic UO_2(s) in the absence of biologic activity. When suspensions of *S. putrefaciens* CN32 cells, Mn oxides

(pyrolusite, birnessite, bixbyite, or a biogenic Mn oxide), U(VI), and H_2 as an electron donor were incubated, the reduction of U(VI) proceeded but was inhibited relative to suspensions without Mn oxide or with gibbsite. These results demonstrate that minor accessory mineral phases in soil or subsurface sediments can affect the in situ bioprecipitation of uranium. Mn(III/IV) oxides in particular may significantly inhibit the microbial reduction of U(VI) and its subsequent precipitation as UO_2(s). Mn oxides are common secondary mineral phases in oxidizing terrestrial environments and are components of soils and sediments at DOE sites where U contamination of the subsurface is significant. Uranium is the most common radionuclide contaminant in groundwaters at DOE sites, and concentrations ranging from 0.001 μg L^{-1} to 11.7 g L^{-1} have been reported. These locations include the Oak Ridge Site in eastern Tennessee and the Hanford Site (Swanson et al., 1999) in south central Washington. Subsurface soils and sediments at Oak Ridge (Arnseth and Turner, 1988) and Hanford (Zachara et al., 1995) contain as much as 0.1 and 1.5% (wt./wt.) dithionite-citrate-bicarbonate-extractable Mn, respectively. Mn oxides (primarily todorokite) associated with Hanford Ringold Formation sediments were implicated in the oxidation of Co(II)$EDTA^{2-}$ to more mobile Co(III)$EDTA^{-}$ in laboratory experiments (Zachara et al., 1995).

A potential mechanism whereby biogenically precipitated UO_2(s) may be physically prevented from contact with Mn oxides is via accumulation in the periplasm of metal-reducing bacterial cells. Although our experiments focused on *S. putrefaciens* CN32, preliminary evidence suggests that UO_2(s) also accumulates in the periplasm of *G. sulfurreducens* cells during the reduction of U (unpublished results), suggesting that this phenomenon may be common in DMRB. *Geobacter* species are believed to be relatively common inhabitants of aquifers (Snoeyenbos-West et al., 2000) and therefore may be relevant organisms for the in situ bioreduction of uranium and other metals. In addition to U(VI), Tc(VII)O_4^{-} that is enzymatically reduced by some DMRB also accumulates as a precipitate in the periplasm (Wildung et al., 2000). Periplasm and cell surface accumulation of U(IV) and Tc(IV) are consistent with current models of enzymatic metal reduction in *Shewanella* and *Geobacter* species.

The impact of mineral precipitation in the periplasm on enzyme function and cell viability is unknown, although on the basis of the TEM images, it appears that CN32 can tolerate relatively high periplasmic concentrations of UO_2(s). As cells age and die or grow and divide, the fate of periplasmic UO_2(s) is difficult to predict. The UO_2(s) may be released as colloids when cells die and lyse. Dividing cells are unlikely to release their periplasmic contents, although Gram-negative bacteria have been known to shed parts of their OM as vesicles (Beveridge, 1999; Kadurugamuwa and Beveridge, 1999). These vesicles may contain periplasmic enzymes (Negrete-Abascal et al., 2000) and presumably could contain mineral precipitate as well. Although we did not observe membrane vesicles in our studies, they are present in CN32 cultures (Y. Gorby, personal communication). The periplasmic precipitation of U (and Tc) is intriguing and potentially significant to in situ contaminant stabilization and warrants further investigation with regard to the postreduction fate of reduced biominerals.

Fe(III) oxides are often in equal or greater abundance in soils and sediments than Mn(III/IV) oxides and may also affect the fate of U during bioreduction. The presence of ferrihydrite, probably because of its poorly crystalline nature and relative availability as an electron acceptor, inhibits bacterial U reduction (Wielinga et al., 2000). However, the crystalline goethite has little effect (Fredrickson et al., 2000; Wielinga et al., 2000). More recently, biogenic Fe(II) associated with solid phases has been shown to indirectly reduce U(VI) (Fredrickson et al., 2000) and Tc(VII) (Lloyd et al., 2000). The fact that Fe(III) and Mn(III/IV) oxides commonly occur in direct association even further complicates the prediction of in situ bioreduction processes. In addition to U(VI), Mn(III/IV) oxides can also oxidize Fe(II). The presence of Mn(III/IV) oxides has been shown to impede the formation of Fe(II) by DMRB (Myers and Nealson, 1988), probably via the rapid oxidation of biogenic Fe(II) (Lovley and Phillips, 1988; Myers and Nealson, 1988; Kostka et al., 1995). Although the extent to which Mn(III/IV) and Fe(III) oxides may jointly affect the in situ microbial reduction of U(VI) is unknown, it is clear that metal reduction and mineral precipitation processes at the cellular level can have an important role.

Acknowledgments—This research was funded by the Natural and Accelerated Bioremediation Research Program, Biological and Environmental Research, DOE. Pacific Northwest National Laboratory is operated for the DOE by the Battelle Memorial Institute under contract DE-AC06-76RLO 1830. Part of this research was supported by Financial Assistance Award DE-FC09-96R18546 from the DOE to the University of Georgia Research Foundation. The X26A microprobe beamline is supported in part by DOE grant DE-FG02-92ER14244. We thank the NSLS staff for assistance. We also wish to thank Paul Gassman for XRD analyses, David Boone (Portland State University) for providing *S. putrefaciens* CN32 to us from the DOE Subsurface Microbial Culture Collection, and Brad Tebo (Scripps Institute of Oceanography) for providing the biogenic Mn(IV) oxide. Finally, the authors wish to thank Ken Nealson, Brad Tebo, and one anonymous reviewer for their insightful review comments.

Associate editor: D. J. Burdige

REFERENCES

Abdelouas A., Lu Y. M., Lutze W., and Nuttall H. E. (1998) Reduction of U(VI) to U(IV) by indigenous bacteria in contaminated ground water. *J. Contam. Hydrol.* **35,** *1–3,* 217–233.

Arnseth R. W. and Turner R. S. (1988) Sequential extraction of iron, manganese, aluminum, and silicon in soils from two contrasting watersheds. *Soil Sci. Soc. Am. J.* **52,** 1801–1807.

Bargar J. R., Tebo B. M., and Villinski J. E. (2000) In situ characterization of Mn(II) oxidation by the spores of the marine Bacillus sp. strain SG-1. *Geochim. Cosmochim. Acta* **64,** 2775–2778.

Beliaev A. S. and Saffarini D. A. (1998) *Shewanella putrefaciens mtrB* encodes and outer membrane proteins required for Fe(III) and Mn(IV) reduction. *J. Bacteriol* **180,** 6292–6297.

Beveridge T. J. (1999) Structures of gram-negative cell walls and their derived membrane vesicles. *J. Bacteriol.* **181,** *16,* 4725–4733.

Burdige D. J. and Nealson K. H. (1985) Microbial manganese reduction by enrichment cultures from coastal marine sediments. *Appl. Environ. Microbiol.* **50,** 491–496.

Burdige D. J. and Nealson K. H. (1986) Chemical and microbiological studies of sulfide-mediated manganese reduction. *Geomicrobiol. J.* **4,** *4,* 361–387.

Burdige D. J., Dhakar S. P., and Nealson K. H. (1992) Effects of manganese oxide mineralogy on microbial and chemical manganese reduction. *Geomicrobiol. J.* **10,** 27–48.

de Leon J. M., Rehr J. J., Zabinsky S. I., and Albers R. C. (1991) *Ab initio* curved-wave X-ray-absorption fine-structure. *Phys. Rev. B* **44,** *9,* 4146–4156.

Ehrlich H. L. (1987) Manganese oxide reduction as a form of anaerobic respiration. *Geomicrobiol. J.* **5,** 423–431.

Fendorf S. E. and Zasoski R. J. (1992) Chromium(III) oxidation by δ-MnO_2. *Environ. Sci. Technol.* **26,** 79–85.

Fendorf S. E., Zasoski R. J., and Burau R. G. (1993) Competing metal-ion influences on chromium(III) oxidation by birnessite. *Soil Sci. Soc. Am. J.* **57,** *6,* 1508–1515.

Field S. J., Dobbin P. S., Cheesman M. R., Watmough N. J., Thomson A. J., and Richardson D. J. (2000) Purification and magneto-optical spectroscopic characterization of cytoplasmic membrane and outer membrane multiheme c-type cytochromes from *Shewanella frigidimarina* NCIMB400. *J. Biol. Chem.* **275,** *12,* 8515–8522.

Fredrickson J. K., Zachara J. M., Kennedy D. W., Dong H., Onstott T. C., Hinman N. W., and Li S. W. (1998) Biogenic iron mineralization accompanying the dissimilatory reduction of hydrous ferric oxide by a groundwater bacterium. *Geochim. Cosmochim. Acta* **62,** *19/20,* 3239–3257.

Fredrickson J. K., Zachara J. M., Kennedy D. W., Duff M. C., Gorby Y. A., Li S. W., and Krupka K. M. (2000) Reduction of U(VI) in goethite (α-FeOOH) suspensions by a dissimilatory metal-reducing bacterium. *Geochim. Cosmochim. Acta* **64,** 3085–3098.

Gaspard S., Vazquez F., and Holliger C. (1998) Localization and solubilization of the iron(III) reductase of *Geobacter sulfurreducens*. *Appl. Environ. Microbiol.* **64,** *9,* 3188–3194.

Gorby Y. A. and Lovley D. R. (1992) Enzymatic uranium precipitation. *Environ. Sci. Technol.* **26,** *1,* 205–207.

Jardine P. M. and Taylor D. L. (1995) Kinetics and mechanisms of Co(II) EDTA oxidation by pyrolusite. *Geochim. Cosmochim. Acta* **20,** 4193–4203.

Johnson K. S. (1982) Solubility of rhodochrosite ($MnCO_3$) in water and seawater. *Geochim. Cosmochim. Acta* **46,** 1805–1809.

Kadurugamuwa J. L. and Beveridge T. J. (1999) Membrane vesicles derived from *Pseudomonas aeruginosa and Shigella flexneri* can be integrated into the surfaces of other gram-negative bacteria. *Microbiology—UK* **145,** 2051–2060.

Kostka J. E., Luther G. W., and Nealson K. H. (1995) Chemical and biological reduction of Mn(III)-pyrophosphate complexes: Potential importance of dissolved Mn(III) as an environmental oxidant. *Geochim. Cosmochim. Acta* **59,** 885–894.

Kung K.-H. and McBride M. B. (1988a) Electron transfer processes between hydroquinone and hausmannite (Mn_3O_4). *Clays Clay Miner.* **36,** 297–302.

Kung K.-H. and McBride M. B. (1988b) Electron transfer processes between hydroquinone and iron oxides. *Clays Clay Miner.* **36,** 303–309.

Lindsay W. L. (1979) *Chemical Equilibria in Soils*. Wiley-Interscience, New York.

Liu C., Zachara J. M., Fredrickson J. K., Kennedy D. W., and Dohnalkova A. (2002) Modeling the inhibition of the bacterial reduction of U(VI) by β-$MnO_{2(s)}$. *Environ. Sci. Technol.* **36,** 1452–1459.

Lloyd J. R., Sole V. A., Van Praagh C. V. G., and Lovley D. R. (2000) Direct and Fe(II)-mediated reduction of technetium by Fe(III)- reducing bacteria. *Appl. Environ. Microbiol.* **66,** *9,* 3743–3749.

Lovley D. R. (1993) Dissimilatory metal reduction. *Ann. Rev. Microbiol.* **47,** 263–290.

Lovley D. R. and Phillips E. J. P. (1988) Manganese inhibition of microbial iron reduction in anaerobic sediments. *Geomicrobiol. J.* **5,** 145–155.

Lovley D. R. and Phillips E. J. P. (1992) Bioremediation of uranium contamination with enzymatic uranium reduction. *Environ. Sci. Technol.* **26,** 2228–2234.

Lovley D. R., Phillips E. J. P., Gorby Y. A., and Landa E. R. (1991) Microbial reduction of uranium. *Nature* **350,** 413–416.

Lovley D. R., Coates J. D., Blunt-Harris E. L., Phillips E. J. P., and Woodward J. C. (1996) Humic substances as electron acceptors for microbial respiration. *Nature* **382,** 445–448.

Lovley D. R., Fraga J. L., Blunt-Harris E. L., Hayes L. A., Phillips E. J. P., and Coates J. D. (1998) Humic substances as a mediator for microbially catalyzed metal reduction. *Acta Hydrochim. Hydrobiol.* **26,** 152–157.

Luther G. W., Nuzzio D. B., and Wu J. (1994) Speciation of manganese in Chesapeake Bay waters by voltammetric methods. *Anal. Chim. Acta* **284,** 473–480.

Magnuson T. S., Hodges-Myerson A. L., and Lovley D. R. (2000) Characterization of a membrane-bound NADH-dependent Fe^{3+} reductase from the dissimilatory Fe^{3+}-reducing bacterium *Geobacter sulfurreducens*. *FEMS Microbiol. Lett.* **185,** *2,* 205–211.

Mcardell C. S., Stone A. T., and Tian J. (1998) Rection of EDTA and related aminocarboxylate chelating agents with $Co^{III}OOH$ (heterogenite) and $Mn^{III}OOH$ (manganite). *Environ. Sci. Technol.* **32,** 2923–2930.

McCarthy J. and Zachara J. M. (1989) Subsurface transport of contaminants: The role of colloidal particles. *Environ. Sci. Technol.* **23,** 496–502.

McKenzie R. M. (1971) The synthesis of birnessite, cryptomelane, and some other oxides and hydroxides of manganese. *Mineral. Mag.* **38,** 493–502.

McKenzie R. M. (1989) Manganese oxides and hydroxides. *Minerals in Soil Environments*. In: (eds. J. B. Dixon and S. B. Weeds). Soil Science Society of America, Madison, WI, pp. 439–465.

Mohagheghi A., Updegraff D. M., and Goldhaber M. B. (1985) The role of sulfate-reducing bacteria in the deposition of sedimentary uranium ores. *Geomicrobiol. J.* **4,** *2,* 153–173.

Morgan J. J. and Stumm W. (1964) Colloid-chemical properties of manganese dioxide. *J. Coll. Sci.* **19,** 347–359.

Mustre de Leon J., Rehr J. J., Zabinsky S. I., Albers R. C. (1991) *Ab initio* curved-wave X-ray-absorption fine-structure. *Phys. Rev. B* **44,** **9,** 4146–4156.

Myers C. and Myers J. (1997) Outer membrane cytochromes of *Shewanella putrefaciens* MR-1: Spectral analysis, and purification of the 83-kDa *c*-type cytochrome. *Biochim. Biophys. Acta* **1326,** 307–318.

Myers C. R. and Nealson K. H. (1988) Microbial reduction of manganese oxides: Interactions with iron and sulfur. *Geochim. Cosmochim. Acta* **52,** 2727–2732.

Myers C. R. and Myers J. M. (1992) Localization of cytochromes to the outer membrane of anaerobically grown *Shewanella putrefaciens* MR-1. *J. Bacteriol.* **174,** *11,* 3429–3438.

Nealson K. and Myers C. R. (1992) Microbial rediction of manganese and iron: New approaches to carbon cycling. *Appl. Environ. Microbiol.* **58,** 439–443.

Nealson K. and Saffarini D. (1994) Iron and manganese in anaerobic respiration: Environmental significance, physiology, and regulation. *Ann. Rev. Microbiol.* **48,** 311–343.

Nealson K. H. and Ford J. (1980) Surface enhancement of bacterial manganese oxidation: Implications for aquatic environments. *Geomicrobiol. J.* **2,** 21–37.

Negrete-Abascal E., Garcia R. M., Reyes M. E., Godinez D., and de la Garza M. (2000) Membrane vesicles released by *Actinobacillus pleuropneumoniae* contain proteases and Apx toxins. *FEMS Microbiol.* Lett. **191,** *1,* 109–113.

Newman D. K. and Kolter R. (2000) A role for excreted quinones in extracellular electron transfer. *Nature* **405,** *6782,* 94–97.

Newville M., Livins P., Yacoby Y., Rehr J. J., and Stern E. A. (1993) Near-edge X-ray-absorption fine-structure of Pb—A comparison of theory and experiment. *Phys. Rev. B: Condens. Matter* **47,** 14126–14131.

Nico P. S. and Zasoski R. J. (2000) Importance of Mn(III) availability on the rate of Cr(III) oxidation on δ-MnO_2. *Environ. Sci. Technol.* **34,** *16,* 3363–3367.

Nikaido H. (1992) Porins and specific channels of bacterial outer membranes. *Mol. Microbiol.* **6,** 435–442.

Potter R. M. and Rossman G. R. (1979) The tetravalent manganese oxides: Identification, hydration, and structural relationships by infrared spectroscopy. *Am. Mineral.* **64,** 1199–1218.

Rehr J. J. and Albers R. C. (1990) Scattering-matrix formulation of curved-wave multiple-scattering theory—Application to X-ray-absorption fine-structure. *Phys. Rev. B* **41,** *12,* 8139–8149.

Rehr J. J., Deleon J. M., Zabinsky S. I., and Albers R. C. (1991) Theoretical X-ray absorption fine-structure standards. *J. Am. Chem. Soc.* **113,** *14,* 5135–5140.

Ressler T. (1998) WinXAS. A program for X-ray absorption spectroscopy data analysis under MS Windows. *J. Synchro. Rad.* **5,** 118–122.

Robie R. A., Hemingway B. S., Fisher J. R. (1978)Thermodynamic properties of minerals and related substances at 298.15 K and 1 bar (105 pascal) pressure and at higher temperatures. *U. S. Geol. Survey Bull.* **1452**.

Roden E. E. and Zachara J. M. (1996) Microbial reduction of crystalline Fe(III) oxides: Influence of oxide surface area and potential for cell growth. *Environ. Sci. Technol.* **30,** 1618–1628.

Scott D. T., McKnight D. M., Blunt-Harris E. L., Kolesar S. E., and Lovley D. R. (1998) Quinone moieties act as electron acceptors in the reduction of humic substances by humics-reducing microorganisms. *Environ. Sci. Technol.* **32,** 2984–2989.

Smith J. V. and Rivers M. L. (1995) Synchrotron X-ray microanalysis. *Microprobe Techniques in the Earth Sciences*. In: (eds. P. J. Potts, J. F. W Bowles, S. J. B Reed, and M. R. Cave). Chapman & Hall, London, pp. 163–233.

Snoeyenbos-West O. L., Nevin K. P., Anderson R. T., and Lovley D. R. (2000) Enrichment of *Geobacter* species in response to stimulation of Fe(III) reduction in sandy aquifer sediments. *Microb. Ecol.* **39,** *2,* 153–167.

Souff P. and Boulegue J. (1988) Synthetic 10-Å and 7-Å phyllomanganates: Their structures as determined by EXAFS. *Am. Mineral.* **73,** 1162–1169.

Stahl R. S. and James B. R. (1991) Zinc sorption by manganese-oxide-coated sand as a function of pH. *Soil Sci. Soc. Am. J.* **55,** *5,* 1291–1294.

Stern E. A., Newville M., Ravel B., Yacoby Y., and Haskel D. (1995) The UWXAFS analysis package—Philosophy and details. *Physica B* **209,** *1–4,* 117–120.

Stone A. T. and Morgan J. J. (1984) Reduction and dissolution of manganese(III) and manganese(IV) oxides by organics. 1. Reaction with hydroquinone.. *Environ. Sci. Technol.* **18,** 450–456.

Stone A. T. and Ulrich H. (1989) Kinetics and reaction stoichiometry in the reductive dissolution of manganese(IV) dioxide and Co(III) oxide by hydroquinone. *J. Colloid Interface Sci.* **132,** 509–522.

Swanson L. C., Rohay V. J., and Faurote J. M. (1999) *Hydrogeologic Conceptual Model for the Carbon Tetrachloride and Uranium/Technetium Plumes in the 200 West Area: 1994 Through 1999 Update*. Bechtel Hanford, Inc., Richland, WA.

Truex M. J., Peyton B. M., Valentine N. B., and Gorby Y. A. (1997) Kinetics of U(VI) reduction by a dissimilatory Fe(III)-reducing bacterium under non-growth conditions. *Biotechnol. Bioeng.* **555,** 490–496.

Wielinga B., Bostick B., Hansel C. M., Rosenzweig R. F., and Fendorf S. (2000) Inhibition of bacterially promoted uranium reduction: Ferric (hydr)oxides as competitive electron acceptors. *Environ. Sci. Technol.* **34,** *11,* 2190–2.

Wildung R. E., Gorby Y. A., Krupka K. M., Hess N. J., Li S. W., Plymale A. E., McKinley J. P., and Fredrickson J. K. (2000) Effect of electron donor and solution chemistry on the products of the dissimilatory reduction of technetium by. *Shewanella putrefaciens* **66,** 2451–2460.

Zachara J. M., Gassman P. L., Smith S. C., and Taylor D. (1995) Oxidation and adsorption of Co(II) $EDTA^{2-}$ complexes in a subsurface materials with iron and manganese oxides. *Geochim. Cosmochim. Acta* **59,** 4449–4463.

Zachara J. M., Fredrickson J. K., Li S. W., Kennedy D. W., Smith S. C., and Gassman P. L. (1998) Bacterial reduction of crystalline Fe^{3+} oxides in single phase suspensions and subsurface materials. *Am. Mineral.* **83,** 1426–1443.